Structure and Dynamics of Lipoplex Formation Examined Using Two-Photon Fluorescence Cross-Correlation Spectroscopy†

Dennis Merkle,‡,§ Susan P. Lees-Miller,§ and David T. Cramb*,‡

Department of Chemistry, University of Calgary, 2500 University Drive, NW, Calgary, Alberta T2N 1N4, Canada, and Department of Biochemistry and Molecular Biology, University of Calgary, 3300 Hospital Drive, Calgary, Alberta T2N 4N1, Canada

Received November 26, 2003; Revised Manuscript Received April 7, 2004

ABSTRACT: The conditions required to form transfectable lipoplexes have been extensively studied [Zuhorn, I. S., and Hoekstra, D. (2002) *J. Membr. Biol. 189*, 167−179]. However, to date, experiments have not addressed either the order of events of lipoplex formation in solution or the maximum number of DNA molecules per vesicle in stable single-vesicle lipoplexes. In this study, we have employed two-photon excitation fluorescence correlation spectroscopy (TPE-FCS) and two-photon fluorescence cross-correlation spectroscopy (TPE-XCS) to examine both fluorescence-labeled DNA and cationic vesicle structure and dynamics simultaneously. The dependence of large aggregated lipoplex formation on DNA-to-cationic lipid charge ratio was determined, as was the maximum number of 40 bp double-stranded DNA oligonucleotides able to bind to a single vesicle.

While viral gene therapy possesses promising clinical application, with high transfection efficiencies, the possibility of unwanted immunological responses and mutagenesis has stimulated investigations of nonviral gene delivery methods. The dominant nonviral delivery vehicles for gene therapy are polymers and cationic lipids. Favorable electrostatic interactions drive complex formation between the DNA and lipids or polymers to form lipoplexes and polyplexes, respectively. Using appropriate lipoplex assemblies, the charged surface of the cationic lipid vesicles also ensures interaction with the negatively charged target cell surface. This step is critical for successful cellular entry of the lipoplex, which is the initial step in transfection.

Lipoplexes form when counterions from the lipid surface are displaced by DNA and either the lipid vesicle collapses onto the DNA or vice versa. Various studies examining the mechanisms of association between cationic lipids and DNA have revealed a variety of factors which can be manipulated to give rise to a variety of supramolecular structures (*1*). Such factors include the fluidity of the cationic lipids, molar charge ratios between DNA (negative) and lipids (positive), the order of component addition (i.e., DNA to lipids or lipids to DNA), and the presence of helper lipids, salts, and other cellular components. Conditions that promote the formation of large lipoplex aggregates have been shown to possess higher transfection activity (*2*). Ensuring the proper mixing of the components in the presence of a positive molar charge ratio, of cationic lipid to DNA, promotes the formation of such transfectionally active lipoplex aggregates (*3*).

There has been a wide range of studies examining the structure and formation of transfectable lipoplexes, including calorimetric analysis (*4*), cryoelectron imaging (*5*, *6*), and dynamic light scattering (*4*). Unfortunately, such studies may be limited due to the fact that they often require conditions that are not physiologically relevant. These previous studies have also failed to elucidate exactly how much DNA is capable of lipid interaction during lipoplex formation. Fluorescence techniques provide an excellent alternative due to the fact that they can be used under physiological conditions, while the individual labeling of DNA and lipid allows for dynamic and time-resolved examination of their interaction in solution.

Recently, studies using fluorescence resonance energy transfer (FRET)[1] (*7*) and fluorescence correlation spectroscopy (FCS) (*8*, *9*) have examined DNA interactions with both polymers (*7*−*9*) and lipids (LipofectAMINE) (*7*). These studies were limited by the fact that they monitored a single species at a time. As an alternative, two-photon excitation

† This work was funded through operating grants from the Natural Sciences and Engineering Research Council and the Canadian Institute for Photonics Innovation (to D.T.C.) and the National Cancer Institute of Canada and the Alberta Cancer Board (to S.P.L.-M.). S.P.L.-M. is a Heritage Medical Scientist of the Alberta Heritage Foundation for Medical Research and an Investigator of the Canadian Institutes for Health Research and holds the Alberta Cancer Foundation/Engineered Air Chair in Cancer Research. D.M. was supported by a studentship through the Alberta Cancer Board.

* To whom correspondence should be addressed: Department of Chemistry, University of Calgary, 2500 University Dr., NW, Calgary, AB T2N 1N4, Canada. Phone: (403) 220-8138. Fax: (403) 289-9488. E-mail: dcramb@ucalgary.ca.

‡ Department of Chemistry.

§ Department of Biochemistry and Molecular Biology.

[1] Abbreviations: CR, charge ratio; DLS, dynamic light scattering; DOTAP, 1,2-dioleoyl-3-trimethylammonium propane; DOTAPf, DOTAP labeled with fluorescein-DHPE; DOTAPl, DOTAP labeled with lissamine-DOPE; FCS, fluorescence correlation spectroscopy; fluorescein-DHPE, *N*-(fluorescein-5-thiocarbamoyl)-1,2-dihexadecanoyl-*sn*-glycero-3-phosphoethanolamine; FRET, fluorescence resonance energy transfer; ITC, isothermal calorimetry; lissamine-DOPE, lissamine dioleoylphosphatidylethanolamine; SUV, single unilamellar vesicle; TPE, two-photon excitation; XCS, fluorescence cross-correlation spectroscopy.

10.1021/bi036133p CCC: $27.50
Published on Web 05/18/2004

(TPE) fluorescence cross-correlation spectroscopy (XCS) allows for the time-resolved correlation of fluorescence signals from two separate color channels. As a result, only when the two differing color fluorophores are interacting do their signals cross-correlate (*10*). Hence, the fluorescence labeling of both DNA and lipid vesicles allows for their simultaneous detection and cross-correlation. TPE is advantageous due to its highly defined excitation volume and high signal-to-scattered light ratios (*11*).

The work presented here examines, by TPE fluorescence spectroscopy, TPE-XCS, and TPE-FCS, the interactions of a 40 bp oligonucleotide with the cationic lipid, DOTAP. By utilizing a red fluorescence label on the 40 bp oligonucleotide and both red and green fluorescence labels on DOTAP small unilamellar vesicles (SUVs), it is possible to examine both labeled DNA and labeled DOTAP interactions as well as aggregation of the lipid vesicles in the presence and absence of unlabeled 40 bp DNA. This allows for the elucidation of the number of 40 bp DNA molecules per lipid vesicle, in the absence of aggregation, as well as revealing a heterogeneous distribution of lipoplex aggregate sizes. To the best of our knowledge, no lipoplex formation studies have been performed using such short oligonucleotides. Double-stranded 40 bp DNA was utilized for these experiments in favor of plasmid DNA, because 40 bp double-stranded DNA is ridged and lacks any secondary DNA structure. In many ways, it is modeled well as a charged cylinder. This allows for a more accurate examination of how much DNA will interact with the positive surface of the lipid vesicle since all the negative charge is exposed on the DNA surface and not buried in any highly supercoiled structures, as is the case in plasmid DNA. Moreover, the surface area per oligonucleotide is easily calculated. We extend these studies to demonstrate that lipoplex formation in solution is a dynamic, two-step process that involves the condensation of the DNA onto the vesicle surface prior to vesicle aggregation.

MATERIALS AND METHODS

Cationic Lipid. DOTAP (1,2-dioleoyl-3-trimethylammonium propane) was obtained from Avanti Polar Lipids (Alabaster, AL).

Fluorescence Labels for Lipids. Fluorescein-DHPE [*N*-(fluorescein-5-thiocarbamoyl)-1,2-dihexadecanoyl-*sn*-glycero-3-phosphoethanolamine, trimethylammonium salt] and Lissamine-DOPE (dioleoylphosphatidylethanolamine) were obtained from Molecular Probes (Eugene, OR).

40 bp Oligonucleotide. Complementary linear, 40-base deoxyoligonucleotides were synthesized at The University of Calgary DNA Synthesis Lab: 5′-CCAGTGAATTGTAATACGACTCACTATAGGGCGAATTGGG-3′ (strand A) and 5′-CCCAATTCGCCCTATAGTGAGTCGTATTACAATTCACTGG-3′ (strand B). Strand A was synthesized with a 5′ amino modification to allow for fluorescence labeling.

Fluorescence Labels for DNA. Labeling of the 40 bp oligonucleotide was accomplished using the Alexa Fluor 594 Oligonucleotide Amine Labeling Kit from Molecular Probes.

Preparation and Fluorescence Labeling of DOTAP. DOTAP was stored as a 3.6 mM stock in chloroform. Fluorescein-DHPE was stored as a 4.23×10^{-4} M stock in chloroform, and Lissamine-DOPE was stored as a 7.68×10^{-5} M stock in methanol. DOTAP vesicles were prepared by evaporation of 100 μL of the 3.6 mM DOTAP stock with nitrogen gas which forms a dry lipid film inside a 5 mL volumetric flask. The film was then resuspended to 5 mL with 50 mM TRIS buffer (pH 8.0). The contents were vigorously stirred for 30 min at room temperature followed by four cycles of sonication for 10 min and stirring for 10 min at room temperature, and the lipids were stored at 4 °C for a maximum of 5 days until they were used. Prior to being used, the DOTAP solution underwent three cycles of stirring for 10 min followed by sonication for 10 min at room temperature and then was then extruded six times through a 100 nm polycarbonate filter in 500 μL aliquots, using an Avanti mini-extruder (Avanti Polar Lipids). Suspensions were used immediately. In the case of fluorescein-DHPE-labeled DOTAP, 5 μL of a 4.23×10^{-4} M stock was mixed into 100 μL of a 3.6 mM DOTAP stock in chloroform prior to evaporation with nitrogen gas. The procedure described above is then followed as outlined. In the case of lissamine-DOPE-labeled DOTAP, 15 μL of a 7.68×10^{-5} M stock was mixed into 100 μL of the 3.6 mM DOTAP stock in chloroform prior to evaporation with nitrogen gas. The procedure described above was then followed.

DNA Strand Annealing and Fluorescence Labeling. Twenty-five micrograms of each 40-base oligonucleotide (1 mg/mL stock of each strand) was added to a final volume of 500 μL in 10 mM TRIS (pH 8), 1 mM EDTA, and 50 mM NaCl. The solution was mixed gently, placed in a 90 °C heating block, and then left to cool to room temperature over the course of 5 h. This produced 50 μg of double-stranded 40 bp linear DNA, which was extracted with phenol and chloroform and precipitated with ethanol. The DNA was fluorescently labeled using the Alexa Fluor 594 Oligonucleotide Labeling Kit (Molecular Probes) following the manufacturer's recommended procedure, and then the labeled 40 bp dsDNA was gel purified using the crush-and-soak method (*12*). Therefore, we are assured of one label per double-stranded oligonucleotide. Experiments involving unlabeled DNA utilize the same 40 bp DNA probe, without the Alexa Fluor 594 labeling reaction. DNA was quantified at 260 nm in a Beckman DU640 UV spectrometer and verified using TPE-FCS. The labeling efficiency was one label per DNA (data not shown).

Lipoplex Formation. Lipoplex assembly was carried out in volumes of 200 μL. In the case of experiments involving labeled DNA and fluorescein-DHPE-labeled DOTAP, 100 μL of extruded labeled DOTAP was thoroughly mixed with a 100 μL mixture of 50 mM TRIS buffer (pH 8) containing well-defined amounts of labeled DNA. Reactions involving dual-labeled DOTAP and unlabeled DNA were carried out by mixing 50 μL of fluorescein-DHPE-labeled DOTAP and 50 μL of lissamine-DOPE-labeled DOTAP. This mixture was then thoroughly mixed into a 100 μL mixture of 50 mM TRIS buffer (pH 8.0) containing various concentrations of unlabeled 40 bp DNA.

FCS and XCS Experimental Setup. In all experiments, the samples were delivered into an eight-well coverslide (Nunc). Samples were excited using 780 nm, 100 fs laser light from a Spectra Physics Tsunami laser operating at 82 MHz. The laser power was attenuated to 20 mW with a neutral density filter to avoid photobleaching. Alexa Fluor 594, fluorescein, and lissamine have reasonable two-photon excitation probability at 780 nm. The laser beam was expanded using a

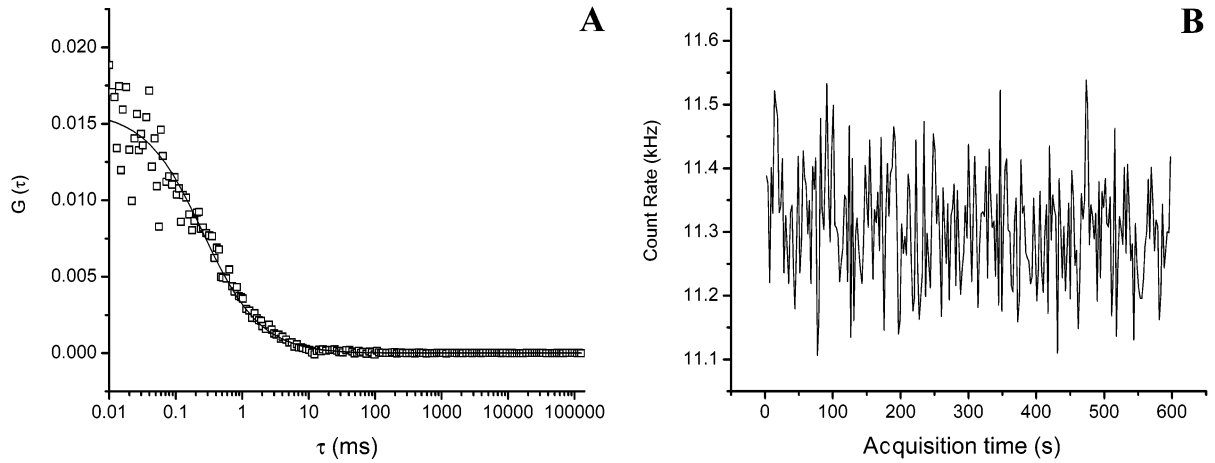

FIGURE 1: Autocorrelation curve (A) and count rate trajectory (B) of Alexa Fluor 594-labeled 40 bp DNA. The empty squares correspond to the experimental signal, while the black line (A) represents the fit to eq 1. The DNA concentration is 120 nM, and the diffusion coefficient, D_{40bp}, is 4.5×10^{-11} m^2/s.

Galilean telescope to slightly overfill the back aperture of a 40×, 0.9 NA Zeiss objective lens mounted on a Zeiss Axiovert 200. TPE fluorescence was collected with the same objective lens, passed through a broad band-pass filter to remove laser light (Omega Optical, XF3100), and reflected off a dichroic optic (Chroma, 700DCSPXR) and through a tube lens in the side port of the microscope. The fluorescence then encounters a second dichroic optic (Chroma 565DCLP) to separate the red and green light. The spectrally separated light passes through band-pass filters (Chroma, E590LPv2 and D535/50x for the red and green emission, respectively) and is coupled into optical fibers located at the focus of the tube lens. Using the optical fibers, the fluorescence is detected by two Si avalanche photodiodes (APDs, Perkin-Elmer, SPCQ-200). The output of the APDs is analyzed using a correlator card (ALV-5000, Langen) installed in a personal computer.

FCS and XCS Data Analysis. Autocorrelation decays were modeled assuming a Gaussian TPE volume using the equation (*10*)

$$G(\tau) = \frac{\left(1 + \frac{8D\tau}{r_0^2}\right)^{-1}\left(1 + \frac{8D\tau}{z_0^2}\right)^{-1/2}}{\langle C\rangle(\pi/2)^{3/2} r_0^2 z_0} \quad (1)$$

where τ is the lag time, D is the diffusion constant, C is the concentration of the diffusing species, r_0 is the laser beam radius at its focus, and z_0 is the depth of focus. The TPE excitation volume was calibrated by measuring the ACF for a 100 nM solution of rhodamine 6G ($D = 2.8 \times 10^{-10}$ m^2/s) in 50 mM TRIS (pH 8.0). The excitation volume was found to be 1.4 fL.

Cross-correlation decays were modeled as described above using the equation (*10*)

$$G_{ij}(\tau) = \frac{\langle C_{ij}\rangle\left(1 + \frac{8D_{ij}\tau}{r_0^2}\right)^{-1}\left(1 + \frac{8D_{ij}\tau}{z_0^2}\right)^{-1/2}}{\langle C_{ij} + C_i\rangle\langle C_{ij} + C_j\rangle(\pi/2)^{3/2} r_0^2 z_0} \quad (2)$$

where subscripts *i*, *j*, and *ij* represent red-labeled, green-labeled, and dual-color-labeled diffusing species, respectively. Nonlinear least-squares fitting to the data was accomplished using Origin.

In some cases, we observed that the correlation decays were best modeled by including a small flow term (*13*):

$$G'(\tau) = G(\tau)e^{-\upsilon^2\tau/4D} \quad (3a)$$

$$G_{ij}'(\tau) = G_{ij}(\tau)e^{-\upsilon^2\tau/4D} \quad (3b)$$

where υ is the flow velocity in meters per second. Since the flow ($\sim 6 \times 10^{-6}$ m/s) is only slightly greater than the Brownian velocity, the value of $G(0)$ is not affected. Under our conditions, only the longer lag times of the correlation decays are affected by flow. This flow was observed for highly charged vesicles such as pure DOPTAP (and carboxylated polystyrene spheres) and did not depend on laser intensity. We attributed the flow to the Marangoni effect (*14*) in which the flow is induced by an ionic strength gradient near the chamber surface.

Dynamic Light Scattering (DLS) of Vesicle Solutions. DLS experiments were performed using a Brookhaven instrument (Brookhaven, CT) on the vesicle preparations at a scattering angle of 90°. The light scattering data were analyzed following the method of cumulants (*15*) to obtain the hydrodynamic radii of the vesicles. The DOTAP vesicles were found to have a radius of 70 ± 10 nm.

RESULTS

FCS Measurements on Free DNA and DOTAP. To establish the behavior of the individual components of lipoplexes, DOTAP SUVs and DNA were examined individually. First, TPE-FCS was performed on free Alexa 594-labeled 40 bp DNA (L-40bp). The resultant autocorrelation decay is plotted in Figure 1A and was fitted to using eq 1. On the basis of a calibrated two-photon excitation volume of 1.4 fL, the diffusion coefficient, D_{40bp}, of the 40 bp DNA was found to be approximately 4.5×10^{-11} m^2/s. The fit also produced a 40 bp DNA concentration of 120 nM, which is in good agreement with 260 nm UV spectroscopic quantification (data not shown). The fluorescence intensity trajectory for the labeled DNA is displayed in Figure 1B.

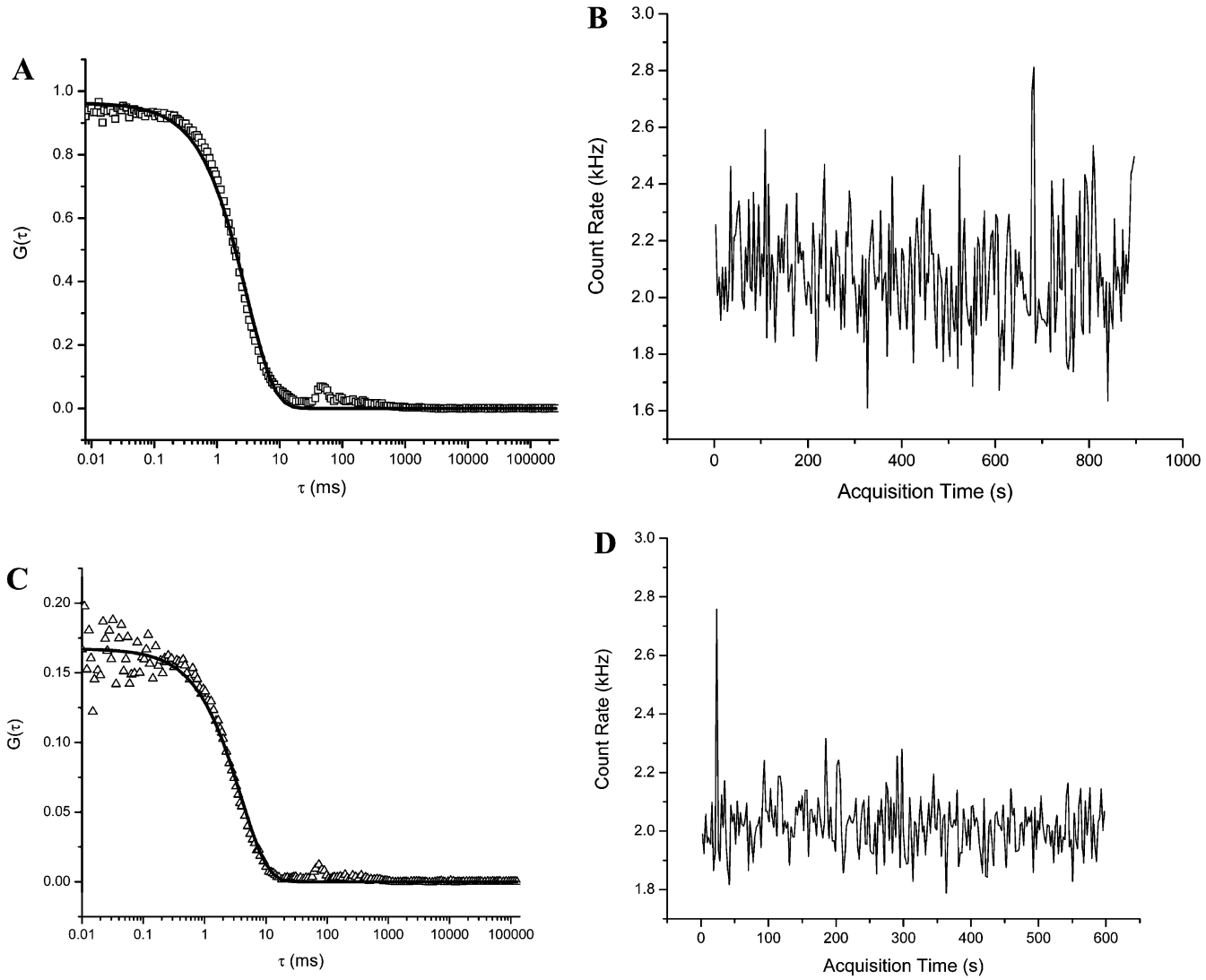

FIGURE 2: Autocorrelation curves of fluorescein-DHPE-labeled (A) and lissamine-DOPE-labeled (C) DOTAP (DOTAPf and DOTAPl, respectively). Lines refer to the fit produced by eq 3a, while the empty squares and triangles correspond to the fluorescein and lissamine experimental signals, respectively. The concentrations of DOTAPf and DOTAPl are 1 and 5.8 nM, respectively, while both labeled DOTAP vesicles exhibit a diffusion coefficient of approximately 2.1×10^{-12} m^2/s. Corresponding count rate trajectories of DOTAPf (B) and DOTAPl (D) are also shown.

Next, TPE-FCS was carried out on DOTAP SUVs labeled with fluorescein-DHPE (DOTAPf) and DOTAP SUVs labeled with lissamine-DOPE (DOTAPl). The concentration of the extruded DOTAPf vesicles was approximately 1 nM from the fit using eq 3a (Figure 2A), while the diffusion coefficient of the DOTAPf vesicles, D_f, was calculated to be 2.1×10^{-12} m^2/s. The concentration of the extruded DOTAPl vesicles was approximately 5.8 nM (Figure 2C), while the diffusion coefficient of the DOTAPl vesicles, D_l, was calculated also to be 2.1×10^{-12} m^2/s. Using the Stokes−Einstein equation, a vesicle diameter of 140 nm was calculated from these diffusion coefficients, which agrees nicely with the result from DLS. Note that in many correlation decays, small peaks appear between lag times of 20 and 1000 ms. This is an artifact due to multiple reflections through the coverslip of the sample chamber and is not included in the fitting. The correlated signal appears to be due to the 50−60 Hz powerline fluctuations. In panels B and D of Figure 2, the fluorescence trajectories for DOTAPf and DOTAPl SUVs, respectively, are shown.

XCS Measurements of Mixed Fluorescein- and Lissamine-Labeled DOTAP in the Presence of Unlabeled DNA. It has been shown that a critical factor in DNA-promoted vesicle aggregation is the molar charge ratios of lipid (+'ve) to DNA (−'ve) (*1*). To define the parameters that dictate DOTAP vesicle aggregation, in the presence of 40 bp linear DNA, TPE-XCS was performed on a mixture of fluorescein-DHPE- and lissamine-DOPE-labeled DOTAP in the presence of a series of 40 bp DNA concentrations. We found that 40 bp DNA induces aggregation of DOTAP when the positive-to-negative charge ratio > 4. Figure 3 shows fluorescence count rate trajectories of the mixed fluorescein- and lissamine-labeled DOTAP vesicles in the absence (A) and presence (B−D) of DNA. In the absence of DNA, there is a steady signal-to-noise ratio from both channels. The concentrations of the fluorescein- and lissamine-labeled DOTAP vesicles are 1 and 2.5 nM, respectively, yielding an overall DOTAP vesicle concentration of 3.5 nM. Concentrations were calculated by fitting to the autocorrelation decay functions produced by each labeled DOTAP species separately, as in

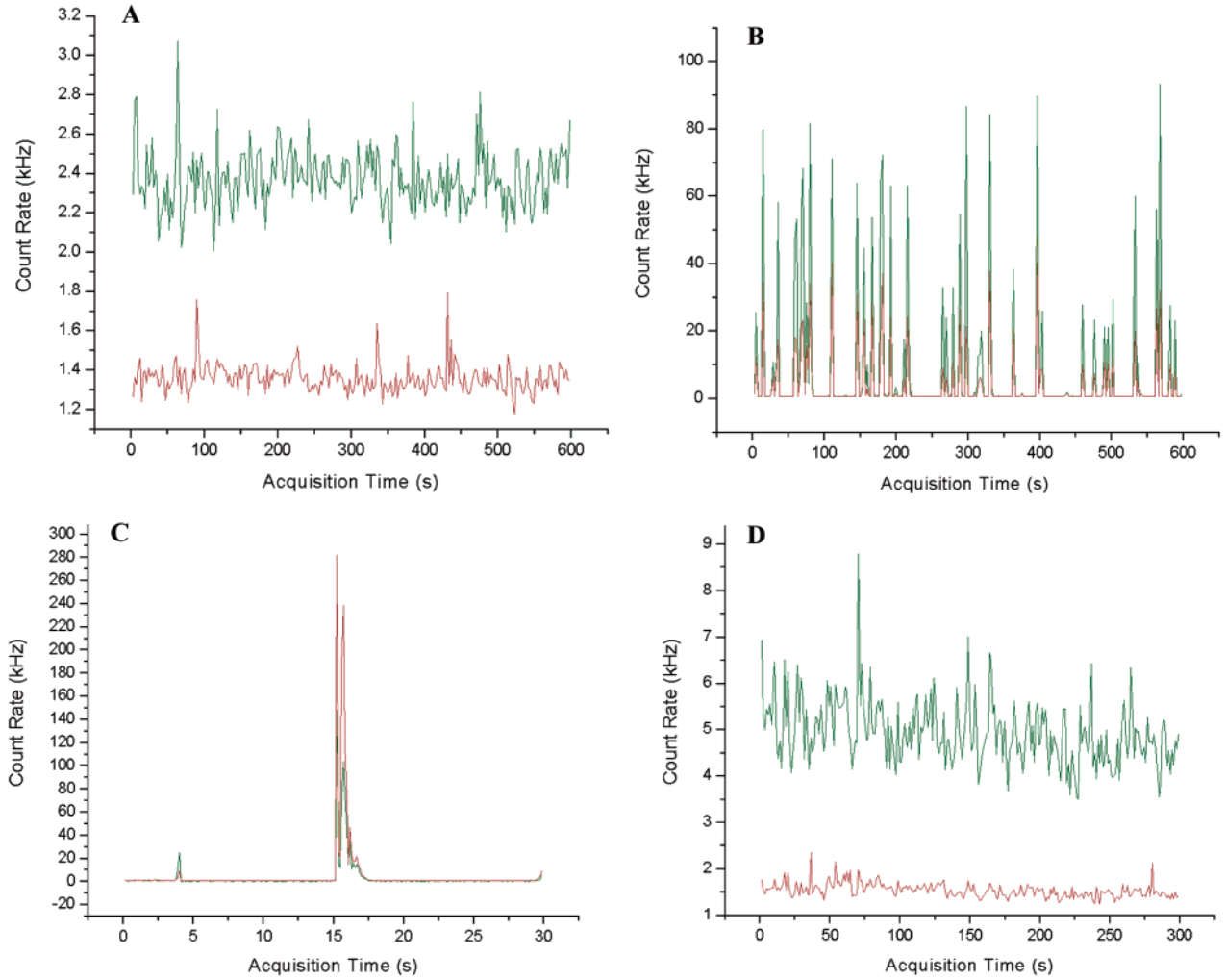

FIGURE 3: Simultaneous dual-channel count rate trajectories of DOTAPf (green) and DOTAPl (red) mixtures. (A) Dual-labeled DOTAP mix in the absence of DNA. (B−D) Dual-labeled DOTAP mix with 40 bp DNA at a positive-to-negative molar charge ratio of (B) 8.75:1 (DNA concentration of 500 nM), (C) 5.5:1 (DNA concentration of 790 nM), and (D) 1.6:1 (DNA concentration of 1406 nM). In panels A−C, the concentration of the DOTAPf vesicles is 1 nM while the concentration of the DOTAPl vesicles is 2.5 nM (total vesicle concentration of 3.5 nM). In panel D, the concentrations for the fluorescein- and lissamine-labeled DOTAP vesicles are 0.5 and 1.25 nM, respectively (total vesicle concentration of 1.75 nM).

Figure 2 (using eq 3a, data not shown). When the positive-to-negative molar charge ratio > 4 (Figure 3B,C), one notes the presence of highly correlated fluorescence count rate trajectories, attributed to the presence of multi-DOTAP vesicle aggregates. In Figure 3B, the positive-to-negative charge ratio is 8.8, whereas in Figure 3C, the ratio is 5.5. The intensity of the peaks ranges from 2 to 200 times larger than the signal for single SUVs. The brightness for a single SUV is calculated from the average count rate under DNA free conditions (Figure 2). Here the concentration of SUVs in the excitation volume is determined directly from analysis of the autocorrelation decays (Figure 2). Also, as the vesicles begin to associate (Figure 3B,C), the background intensities of each labeled species approach 0 kHz, indicating the presence of a smaller number of emitting species in the excitation volume. The large peaks in the red channel often overlap with large peaks in the green channel, demonstrating large DOTAP aggregates that contain multiple fluorescein- and lissamine-labeled vesicles. The wide variation in the peak intensity is also indicative of a wide distribution of sizes of the aggregates, which makes analysis of the cross-correlation curve very challenging. Nevertheless, association between vesicles is clearly shown in Figure 4, where the TPE cross-correlation decays for SUV association in the absence and presence of DNA are displayed. The inset of Figure 4 shows that a small amount of background cross-correlation results from cross talk of the green probe detected in the red channel. As the positive-to-negative molar charge ratio approaches unity (Figure 3D), the frequency and intensity of the peaks decrease. These results are in good agreement with the previously defined positive-to-negative molar charge ratios that dictate vesicle−DNA aggregation (*1*). Additionally, these results indicate that short oligonucleotides (40 bp) promote qualitatively the same lipoplex characteristics as larger DNA (≥3 kb) (*16*).

Lipoplex Formation near the Balanced Charge Regime. Despite the fact that there was no large vesicle aggregation at molar charge ratios that approach unity, there are still some vesicle association events. Figure 5A is a frequency count analysis of a 5 min count rate trajectory for a 1 nM DOTAPf solution. A single Gaussian count distribution, centered at 2.1 kHz, indicates the dominance of single diffusing DOTAP vesicles. The Gaussian distribution is an approximation used to compare the count rate distribution between different

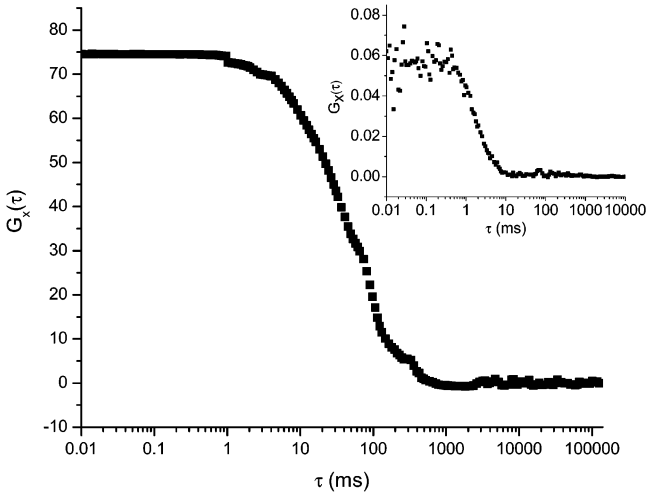

FIGURE 4: Cross-correlation decay [$G_x(\tau)$] (black) of a mixture of DOTAPf (1 nM) and DOTAPl (2.5 nM) in the presence of 500 nM unlabeled 40 bp DNA. The count rate trajectory for this mixture is presented in Figure 3B. The inset shows the $G_x(\tau)$ of the mixture of DOTAPf and DOTAPl in the absence of DNA, the trajectory of which was depicted in Figure 3A. The non-zero $G_x(0)$ in the inset results from slight cross talk of the green probe in the red detector channel.

sample conditions. Our limited fluorescence collection bin size did not permit application of the photon counting trajectory analysis approach (*17*). Compare this with Figure 5B, which is a frequency count analysis of a 5 min count rate trajectory of 0.5 nM DOTAPf in the presence of 1000 nM DNA (1:1.6 positive-to-negative molar charge ratio). Since this solution contained only half the amount of DOTAPf used in the previous experiment (Figure 5A), the fluorescence signal of the DOTAPf count rate trajectory used in Figure 5B was normalized to that of the count rate trajectory used in Figure 5A, solely for visual comparison in the figure. It is evident (Figure 5B) that in the presence of DNA, in a regime that does not result in formation of large DOTAP aggregates, there is no longer a single diffusing species. Instead of a clear single Gaussian distribution centered near 2.1 kHz (as in Figure 5A), there is a distribution of diffusing populations from 2 to 5 kHz. This result suggests that DNA causes some degree of vesicle association, even in the presence of excess negative charge. The 2−5 kHz range of fluorescence count rates (Figure 5B) suggests a distribution of single DOTAP vesicles (∼2 kHz) as well as pairs of DNA-induced, associated vesicles (∼4 kHz).

As indicated above, at positive-to-negative molar charge ratios of >4, large DNA−DOTAP aggregates were formed, which possess a large distribution of sizes. As the molar charge ratio approaches unity, no large aggregates were formed, although there was still some pairwise association of the vesicles. These results are in good agreement with cryoelectron microscopy studies (*6*) that show similar large vesicle aggregates at positive molar charge ratios of >4 and a lack of such aggregates at charge ratios near unity.

Elucidating the Maximum Number of 40 bp DNA Molecules per DOTAP Vesicle. While the parameters dictating lipoplex formation have been well studied, the extent to which DNA interacts with individual vesicles prior to aggregation is less well characterized. To examine how many DNA molecules are capable of interacting with a single DOTAP vesicle, a molar charge ratio near unity was employed.

In an attempt to determine the maximum loading of DNA per DOTAP vesicle, the concentrations of the species were chosen such that vesicle surfaces could be saturated and the formation of multivesicle aggregates minimized. These DNA and SUV concentrations are estimated from the surface area of the SUVs (61 600 nm^2) and the footprint of the cylindrical 40 bp DNA molecules (28 nm^2). Thus, the maximum DNA/SUV ratio can be determined (∼2200), which is the approximate molar ratio that is used. Experiments were performed using both labeled DNA and labeled DOTAP, in which the degree of vesicle association could be assessed, simultaneously with DNA association. Figure 6A shows the autocorrelation function of 0.5 nM DOTAPf vesicles in a solution containing 1000 nM DNA (at a 28:1 molar ratio of unlabeled to labeled DNA, which vastly reduces the likelihood of self-quenching when the DNA condenses onto the SUV). The molar charge ratio of DOTAP to DNA is approximately 1:1.4. In Figure 6A, the green line represents the DOTAPf signal (blue line is the fit to eq 3a). The fit using eq 3a to the DOTAPf channel (blue) results in a concentration of 0.3 nM DOTAP vesicles, which could represent a bimodal size distribution; i.e., there is some association of the original 0.5 nM vesicles. Therefore, 0.3 nM represents an apparent concentration of vesicles. Figure 6B is a cross-correlation analysis of this mixture. The fit of this decay curve to eq 3b (blue) yields a cross-correlated species concentration of 0.3 nM and a free DOTAPf concentration of 0 nM, again indicating that all the DOTAP is DNA-bound. The analysis reveals a free L-40bp DNA concentration of 3.7 nM. Because of the labeled-to-unlabeled DNA ratio (28:1), this would indicate that 104 nM DNA is free in solution. Therefore, approximately 2000 of the 40 bp DNA molecules associate with a single DOTAP vesicle.

Lipoplex Formation Is a Two-Step Process. Lipoplexes form as a result of the electrostatic interactions between the negatively charged DNA and the cationic lipid surface. Although the exact molar charge ratio between DNA and vesicle is known to be a principle factor dictating vesicle aggregation (a necessity for transfectable lipoplexes), the order of events has yet to be elucidated directly from solution studies. In other words, are DNA−vesicle condensation and vesicle aggregation simultaneous processes, or does one event lead to the next? Panels A, D, and G of Figure 7 display the count rate trajectories of 0.5 nM fluorescein-DHPE-labeled DOTAP SUVs in the presence of 72 nM Alexa 594-labeled 40 bp DNA. The fluorescence trajectories were collected over a period of 30 min. Figure 7A demonstrates large peaks in the DNA channel (red) in the first 10 min after mixing of DNA and DOTAP, indicative of multiple-DNA condensation onto the lipid surface (compare with Figure 1B). In contrast, the fluorescence signal from the DOTAPf channel (green) is relatively steady. A normalization of the green channel to that of the red (indicated in blue in panels A, D, and G of Figure 7) was performed to show the extent of DOTAP aggregation in relation to that of the DNA. As indicated by Figure 7D, the period of 10−20 min after mixing of DOTAP and DNA results in the appearance of higher-intensity peaks in the green channel, indicative of DOTAP aggregation. Figure 7G displays the period of 20−30 min after mixing of DOTAP and DNA and demonstrates the appearance of

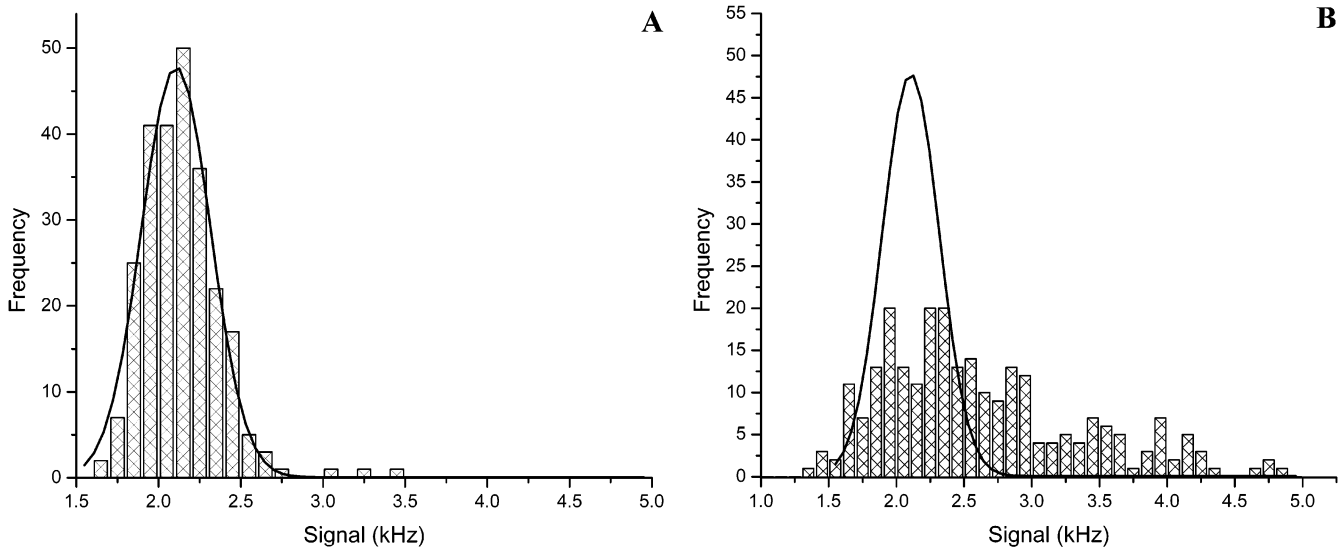

FIGURE 5: Frequency count analysis of count rate trajectories of a 1 nM DOTAPf solution (A) and a 0.5 nM DOTAPf solution containing 1725 nM DNA (B). The signal intensity of the count rate trajectory used in panel B was normalized to that of panel A. The line is a Gaussian distribution function fitted to the data in panel A and is transposed onto the data in panel B for comparison.

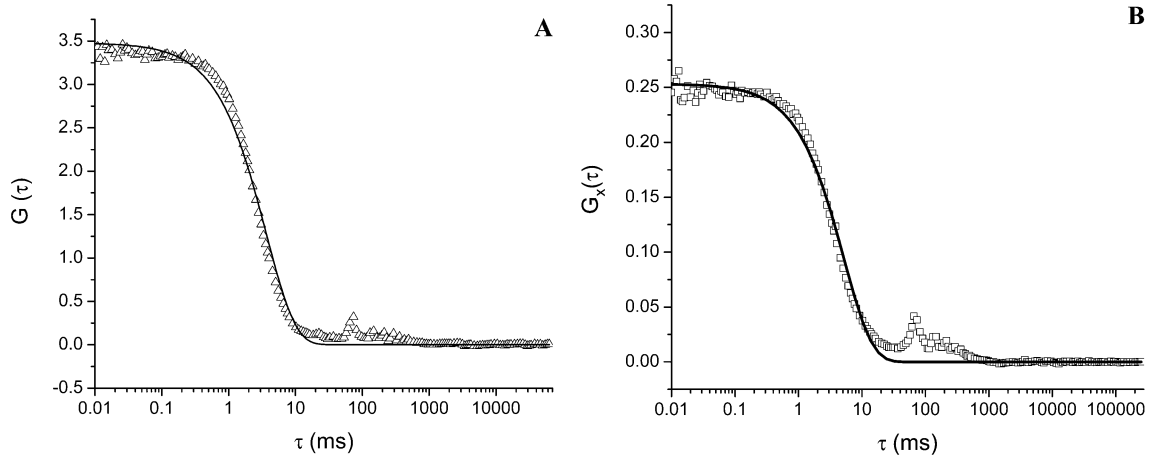

FIGURE 6: Fluorescence correlation analysis of a 0.5 nM DOTAPf solution containing 1000 nM DNA (at a 28:1 molar ratio of unlabeled 40 bp DNA to L-40bp). (A) Autocorrelation function of the DOTAPf signal (△) fitted using eq 3a (black line). (B) Cross-correlation function (□) of both green and red channels fitted using eq 3b (black line).

even higher-intensity peaks in both channels, suggesting the formation of increasingly large lipoplexes.

Figure 7B (0−10 min), Figure 7E (10−20 min), and Figure 7H (20−30 min) are intensity frequency counts of the normalized green (DOTAPf) channel [blue line(s)] from 0 to 20 kHz in 0.5 kHz intervals. The initial 10 min period (Figure 7B) after mixing of DOTAP and DNA results in a dominant DOTAPf signal distribution around 2−3 kHz. These fluorescence intensity trajectories are representative of results consistently observed over several experiments. Frequency counts of larger intensity events (i.e., 20−200 kHz peaks) are plotted in Figure 7C (0−10 min), Figure 7F (10−20 min), and Figure 7I (20−30 min). Only three events on the order of 20 kHz are seen within the first 10 min of mixing (Figure 7C), while this number increases to 9 after 20 min (Figure 7F) and up to 12 after 30 min (Figure 7I). Figure 7D and Figure 7G also display events on the order of 50−160 kHz showing that large aggregation of the lipid vesicles does not occur until ∼10 min after mixing of the DOTAP/DNA solution. In contrast, the DNA channel (red lines, Figure 7A,D,G) shows large peaks in intensity within 1 min of mixing of DOTAP and DNA. In all, these data show that lipoplex formation is a dynamic two-step process that involves an initial, faster condensation of DNA on the vesicle prior to vesicle aggregation.

DISCUSSION

There exist numerous studies examining the formation and structure of transfectable lipoplexes. This study utilizes TPE-FCS and TPE-XCS to examine the interactions between a 40 bp oligonucleotide and DOTAP SUVs. These fluorescence techniques allow for dynamic and structural examination of DNA−lipid interactions in solution under physiologically relevant conditions.

Effect of Negative-to-Positive Molar Charge Ratios in Lipoplex Formation. As observed in previous studies (*1*), we found that DNA induces aggregation of DOTAP when the positive-to-negative charge ratio is greater than 4. While previous studies utilize larger plasmid DNA fragments (≥3 kb) (*16*), the 40 bp DNA used in the study presented here promotes qualitatively similar lipoplex aggregation (Figures

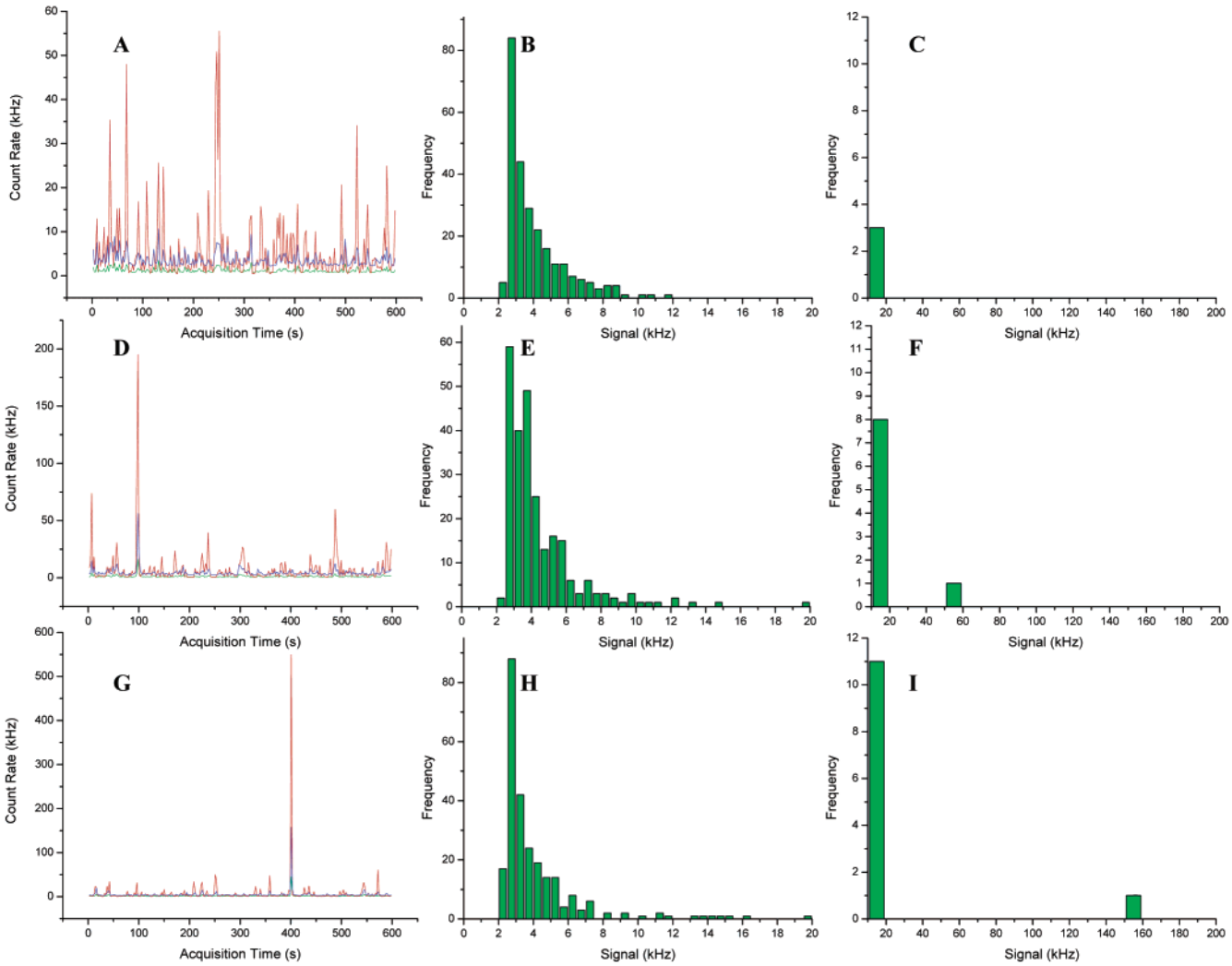

FIGURE 7: Fluorescence count rate trajectories and frequency count analysis of a 0.5 nM DOTAPf solution containing 72 nM L-40bp DNA 10 min after mixing (A−C), 20 min after mixing (D−F), and 30 min after mixing (G−I). Green lines represent the signal of the DOTAPf channel; red lines represent the signal of the L-40bp DNA channel, and the blue lines are normalizations of the background of the green channel to that of the red. The normalized signals (blue) are used for the frequency count analysis in panels B, C, E, F, H, and I.

3 and 4). Although there was no large vesicle aggregation at molar charge ratios that approach unity, some mixing of lipid vesicles still takes place (Figure 5). That is, a balanced charge ratio does not promote the formation of large lipoplex aggregates, nor does the charge balance result in a single diffusing species of DOTAP SUVs.

Elucidating the Maximum Number of 40 bp DNA Molecules per DOTAP Vesicle near Charge Balance. To examine how many DNA molecules are capable of interacting with a single DOTAP vesicle, a molar charge ratio near unity was employed. The 40 bp oligonucleotide with a single 5′ amino modification was favorable due to its ridged structure, ensuring that all the negative charge is exposed on the DNA surface. Additionally, because each DNA molecule can only facilitate one fluorescence label, the average count rate per DNA molecule can be determined. From Figure 1, an average of 67 DNA molecules occupy the TPE volume and produce an average count rate of 11.4 kHz. This results in an average signal of 170 Hz per L-40bp DNA molecule. If its is assumed that a DOTAP vesicle is approximately 140 nm in diameter (as derived from the diffusion coefficients via the Stokes−Einstein relationship and from dynamic light scattering), it would possess a surface area of approximately 61 600 nm^2. A 40 bp double-stranded B-form DNA molecule is approximately 14 nm in length and approximately 2 nm in thickness. This translates to a 28 nm^2 area footprint per 40 bp DNA molecule. If DNA coats only the outer surface of a 140 nm diameter vesicle with the tightest possible packing, a yield of approximately 2200 DNA molecules per vesicle would be possible. If the DNA instead sweeps out a circular area (with a diameter equivalent to its length, 14 nm), then each DNA molecule would occupy an approximate 154 nm^2 area, and hence, approximately 400 DNA molecules would coat the outer surface of a 140 nm diameter vesicle. The DNA is unlikely to maximally coat the vesicle (2200 DNA molecules per vesicle) due to entropic limitations; however, it is also unlikely that a completely evenly distributed minimal loading of DNA occurs (i.e., 400 DNA molecules per vesicle). Therefore, the maximum that we observe, ~2000 40 bp DNA molecules, is a reasonable compromise between packing efficiency and entropy. Recall that the maximum we calculated was for excess DNA and that free DNA was observed under these conditions (i.e., charge ratio near unity). Also, since there is some association of liposomes, even in the presence of excess negative charge (Figure 5), it is not

unreasonable to record events with more than 2000 DNA molecules per diffusing lipoplex.

It should be noted that the diffusion coefficients produced from the fits of eqs 3a and 3b to the data in Figure 6 do suggest larger diffusing species. The approximate diffusion coefficients of the free L-40bp and free DOTAP are 4.5×10^{-11} and 2.1×10^{-12} m^2/s, respectively (Figures 1 and 2), while the fits of the cross-correlated diffusing species in Figure 6 correspond to a species diffusing on the order of 1.8×10^{-12} m^2/s. These values make sense when one considers that the DNA will add only 2 nm to the 70 nm radius of the SUV. There may be an effect on the measured diffusion coefficient, due to the change in the net charge of the lipoplex versus the free SUV; however, we have observed that the difference between extruded zwitterionic dioleoylphosphatidylcholine SUVs (*18*) and DOTAP SUVs is not substantial.

Elucidating the Number of 40 bp DNA Molecules per DOTAP Vesicle under Conditions that Promote Lipoplex Association. It has been previously demonstrated that when the positive-to-negative charge ratio is greater than 4, large aggregated lipoplexes form. It is conceivable that under these conditions, DNA forms a bridge between liposomes and thus has surface packing different from that near charge balance. Since lipoplex formation involves a two-step process (Figure 7), it is possible that the number of DNA molecules per vesicle elucidated above involves multiple vesicles if examined 10 min after mixing of DOTAP and DNA. The maximum peak intensity of L-40bp in the first 10 min is ~50 kHz (Figure 7A). The average background intensity of 72 nM L-40bp is ~6.2 kHz (data not shown), and therefore, the 50 kHz peak is indicative of approximately 300 DNA molecules (40 bp) per vesicle, prior to vesicle aggregation. Therefore, peaks much larger in intensity, suggesting more than 2000 DNA molecules per vesicle, may be indicative of aggregated lipoplexes in the excitation volume. Panels D and G of Figure 7 contain intensity peaks of 200 and 550 kHz in the L-40bp channel. These intensities indicate 1000 and >3000 DNAs per diffusing species in the 200 and 550 kHz peaks, respectively. The normalized intensity of the DOTAPf channel in Figure 7 (blue lines) is around 5−10 kHz in the absence of aggregation (Figure 7A). The 200 and 550 kHz intensity peaks in the DNA channel correspond to approximately 50 and 150 kHz intensity peaks, respectively, in the normalized DOTAPf channel (blue lines in panels D and G of Figure 7). Since the 5−10 kHz signal is representative of approximately 0.5 nM DOTAPf SUVs, the 50 and 150 kHz peaks correspond to aggregates of approximately 3 and 10 vesicles, respectively. Hence, each aggregate still contains approximately 300 DNA molecules per vesicle at a charge ratio of 4:1 (positive to negative).

Current Model of Lipoplex Formation. A working model for lipoplex formation in solution (*12*, *19*) suggests that in most cases, lipoplexes form via at least a two-step process, the first step being condensation of DNA onto cationic vesicles and the second being association of smaller lipoplexes to form larger ones. The second step has been reported to depend on the positive-to-negative charge ratio (CR) (*12*, *19*) and, in some cases, on the order of mixing DNA and lipid (*4*, *20*). The charge dependence of the lipoplex structure (large lipoplexes form when the CR > 4) suggests that DNA bridges cationic vesicles (*16*). Our results are consistent with this interpretation. Moreover, the 40 bp DNA used in our work does not appear to destabilize individual liposomes, consistent with our previous work, which employed atomic force microscopy (*21*). It is, therefore, probable that the large aggregates observed in the current work have had minimal lipid mixing. Additionally, we have observed no dependence of the lipoplex on the order of mixing its components. This is in contrast with isothermal calorimetry (ITC) results (*4*, *20*). However, in ITC a concentrated bolus of either lipid or DNA is microinjected into a solution of the other component, whereas in the current TPE-XCS study, very low concentrations (1−1000 nM) of the components were thoroughly mixed prior to examination.

ACKNOWLEDGMENT

We thank Anna Carnini and Professor Guojun Liu for help with the DLS experiments.

REFERENCES

1. Zuhorn, I. S., and Hoekstra, D. (2002) On the mechanism of cationic amphiphile-mediated transfection. To fuse or not to fuse: is that the question? *J. Membr. Biol. 189*, 167−179.
2. Simberg, D., Danino, D., Talmon, Y., Minsky, A., Ferrari, M. E., Wheeler, C. J., and Barenholz, Y. (2001) Phase behavior, DNA ordering, and size instability of cationic lipoplexes. Relevance to optimal transfection activity, *J. Biol. Chem. 276*, 47453−47459.
3. Rosenweig, H. S., Rakhmanova, V. A., McIntosh, T. J., and MacDonald, R. C. (2000) O-Alkyl dioleoylphosphatidylcholinium compounds: the effect of varying alkyl chain length on their physical properties and in vitro DNA transfection activity, *Bioconjugate Chem. 11*, 306−313.
4. Lobo, B. A., Davis, A., Koe, G., Smith, J. G., and Middaugh, R. C. (2001) Isothermal titration calorimetric analysis of the interaction between cationic lipids and plasmid DNA, *Arch. Biochem. Biophys. 386*, 95−105.
5. Xu, Y., Hui, S. W., Fredrik, P., and Szoka, F. C., Jr. (1999) Physicochemical characterization and purification of cationic lipoplexes, *Biophys. J. 77*, 341−353.
6. Huebner, S., Battersby, B. J., Grimm, R., and Cevc, G. (1999) Lipid-DNA complex formation: reorganization and rupture of lipid vesicles in the presence of DNA as observed by cryoelectron microscopy, *Biophys. J. 76*, 3158−3166.
7. Itaka, K., Harada, A., Nakamura, K., Kawaguchi, H., and Kataoka, K. (2002) Evaluation by fluorescence resonance energy transfer of the stability of nonviral gene delivery vectors under physiological conditions, *Biomacromolecules 3*, 841−845.
8. Clamme, J. P., Azoulay, J., and Mely, Y. (2003) Monitoring of the formation and dissociation of polyethylenimine/DNA complexes by two photon fluorescence correlation spectroscopy, *Biophys. J. 84*, 1960−1968.
9. Kral, T., Hof, M., and Langner, M. (2002) The effect of spermine on plasmid condensation and dye release observed by fluorescence correlation spectroscopy, *Biol. Chem. 383*, 331−335.
10. Heinze, K. G., Koltermann, A., and Schwille, P. (2000) Simultaneous two-photon excitation of distinct labels for dual-color fluorescence crosscorrelation analysis, *Proc. Natl. Acad. Sci. U.S.A. 97*, 10377−10382.
11. Schwille, P., Haupts, U., Maiti, S., and Webb, W. W. (1999) Molecular dynamics in living cells observed by fluorescence correlation spectroscopy with one- and two-photon excitation, *Biophys. J. 77*, 2251−2265.
12. Sambrook, J., Fritsch, E. F., and Maniatis, T. (1989) *Molecular Cloning: A Laboratory Manual*, 2nd ed., Cold Spring Harbor Laboratory Press, Plainview, NY.
13. Goyan, R. L., Paul, R., and Cramb, D. T. (2001) Photodynamics of latex nanospheres examined using two-photon fluorescence correlation spectroscopy, *J. Phys. Chem. B 105*, 2322−2330.
14. Bennett, D. E., Gallardo, B. S., and Abbott, N. L. (1996) Dispensing surfactants from electrodes: Marangoni phenomenon at the surface of aqueous solutions of (11-ferrocenylundecyl)-trimethylammonium bromide, *J. Am. Chem. Soc. 118*, 6499−6505.

15. Ding, J., and Liu, G. (1998) Polystyrene-*block*-poly(2-cinnamoylethyl methacrylate) nanospheres with cross-linked shells, *Macromolecules 31*, 6554−6558.
16. Kennedy, M. T., Pozharski, E. V., Rakhmanova, V. A., and MacDonald, R. C. (2000) Factors governing the assembly of cationic phospholipid-DNA complexes, *Biophys. J. 78*, 1620−1633.
17. Chen, Y., Müller, J. D., So, P. T. C., and Gratton, E. (1999) The Photon Counting Histogram in Fluorescence Fluctuation Spectroscopy, *Biophys. J. 77*, 553−567.
18. Swift, J. S., Carnini, A., Dahms, T. E. S., and Cramb, D. T. (2004) Anesthetic-enhanced Membrane Fusion examined using Two-photon Fluorescence Correlation Spectroscopy, *J. Phys. Chem. B* (in press).
19. Oberle, V., Bakowsky, U., Zuhorn, I. S., and Hoekstra, D. (2000) Lipoplex formation under equilibrium conditions reveals a three-step mechanism, *Biophys. J. 79*, 1447−1454.
20. Pozharski, E., and MacDonald, R. C. (2002) Thermodynamics of cationic lipid-DNA complex formation as studied by isothermal titration calorimetry, *Biophys. J. 83*, 556−565.
21. Leonenko, Z. V., Merkle, D., Lees-Miller, S. P., and Cramb, D. T. (2002) Lipid phase dependence of DNA-cationic phospholipid bilayer interactions examined using atomic force microscopy, *Langmuir 18*, 4873−4884.

BI036133P